Research Article | Vol. 7, No. 5 | 1 May 2017 | OPTICAL MATERIALS EXPRESS 1589

Optical Materials EXPRESS

Laser structuring, stress modification and Bragg grating inscription in silicon-core glass fibers

MICHAEL FOKINE,[1] ANTREAS THEODOSIOU,[2] SEUNGHAN SONG,[3] THOMAS HAWKINS,[4] JOHN BALLATO,[4] KYRIACOS KALLI,[2] AND URSULA J. GIBSON[1,3,*]

[1]*Department of Applied Physics, KTH Royal Institute of Technology, Stockholm, 10044 Sweden*
[2]*Cyprus University of Technology, Department of Electrical Engineering, Computer Engineering and Informatics, Limassol, 3036, Cyprus*
[3]*Department of Physics, Norwegian University of Science and Technology, N-7491 Trondheim, Norway*
[4]*Center for Optical Materials Science and Engineering Technologies (COMSET) and the Department of Materials Science and Engineering, Clemson University, Clemson, SC 29634 USA*
**ursula.gibson@ntnu.no*

Abstract: Semiconductor core fibers have numerous potential applications in optoelectronics and photonics, and the key to realizing these opportunities is controlled processing of the material. We present results on laser treatments for manipulating the core structure as well as the glass cladding. More specifically, using quasi-CW 10.6 μm radiation, the clad glass can be softened and the core can be controllably melted. This is shown to permit tapering, localized formation of optical resonators, and stress modification of the as-drawn fiber and structures within it. Shown for the first time to the authors' knowledge are Bragg gratings written by modification of the silicon/glass interface using fs laser illumination at 517 nm. The cores of these fibers show stress alterations, with indications of quasi-periodic stress relief in the glass.

OCIS codes: (060.2280) Fiber design and fabrication; (060.2390) Fiber optics, infrared; (140.3390) Laser materials processing; (060.3735) Fiber Bragg gratings.

References and links

1. R. He, T. D. Day, M. Krishnamurthi, J. R. Sparks, P. J. A. Sazio, V. Gopalan, and J. V. Badding, "Silicon p-i-n Junction Fibers," Adv. Mater. **25**(10), 1461–1467 (2013).
2. F. A. Martinsen, B. K. Smeltzer, M. Nord, T. Hawkins, J. Ballato, and U. J. Gibson, "Silicon-core glass fibres as microwire radial-junction solar cells," Sci. Rep. **4**, 6283 (2014).
3. F. H. Suhailin, N. Healy, Y. Franz, M. Sumetsky, J. Ballato, A. N. Dibbs, U. J. Gibson, and A. C. Peacock, "Kerr nonlinear switching in a hybrid silica-silicon microspherical resonator," Opt. Express **23**(13), 17263–17268 (2015).
4. P. J. Sazio, A. Amezcua-Correa, C. E. Finlayson, J. R. Hayes, T. J. Scheidemantel, N. F. Baril, B. R. Jackson, D.-J. Won, F. Zhang, E. R. Margine, V. Gopalan, V. H. Crespi, and J. V. Badding, "Microstructured optical fibers as high-pressure microfluidic reactors," Science **311**(5767), 1583–1586 (2006).
5. J. Ballato, T. Hawkins, P. Foy, R. Stolen, B. Kokuoz, M. Ellison, C. McMillen, J. Reppert, A. M. Rao, M. Daw, S. R. Sharma, R. Shori, O. Stafsudd, R. R. Rice, and D. R. Powers, "Silicon optical fiber," Opt. Express **16**(23), 18675–18683 (2008).
6. N. Healy, M. Fokine, Y. Franz, T. Hawkins, M. Jones, J. Ballato, A. C. Peacock, and U. J. Gibson, "CO_2 laser-induced directional recrystallization to produce single crystal silicon-core optical fibers with low loss," Adv. Opt. Mater. **4**(7), 1004–1008 (2016).
7. A. Gumennik, L. Wei, G. Lestoquoy, A. M. Stolyarov, X. Jia, P. H. Rekemeyer, M. J. Smith, X. Liang, B. J.-B. Grena, S. G. Johnson, S. Gradečak, A. F. Abouraddy, J. D. Joannopoulos, and Y. Fink, "Silicon-in-silica spheres via axial thermal gradient in-fibre capillary instabilities," Nat. Commun. **4**, 2216 (2013).
8. S. Chaudhuri, J. R. Sparks, X. Ji, M. Krishnamurthi, L. Shen, N. Healy, A. C. Peacock, V. Gopalan, and J. V. Badding, "Crystalline Silicon Optical Fibers with Low Optical Loss," ACS Photonics **3**(3), 378–384 (2016).
9. X. Ji, S. Lei, S.-Y. Yu, H. Y. Cheng, W. Liu, N. Poilvert, Y. Xiong, I. Dabo, S. E. Mohney, J. V. Badding, and V. Gopalan, "Single-crystal silicon optical fiber by direct laser crystallization," ACS Photonics **4**(1), 85–92 (2017).

#285825 https://doi.org/10.1364/OME.7.001589
Journal © 2017 Received 30 Jan 2017; revised 29 Mar 2017; accepted 29 Mar 2017; published 12 Apr 2017
Corrected: 18 April 2017

Optical Materials EXPRESS

10. N. Healy, S. Mailis, N. M. Bulgakova, P. J. A. Sazio, T. D. Day, J. R. Sparks, H. Y. Cheng, J. V. Badding, and A. C. Peacock, "Extreme electronic bandgap modification in laser-crystallized silicon optical fibres," Nat. Mater. **13**(12), 1122–1127 (2014).
11. X. Ji, R. L. Page, S. Chaudhuri, W. Liu, S.-Y. Yu, S. E. Mohney, J. V. Badding, and V. Gopalan, "Single-Crystal Germanium Core Optoelectronic Fibers," Adv. Opt. Mater. **5**, 1600592 (2017).
12. P. Holmberg and M. Fokine, "Thermometric study of CO_2-laser heated optical fibers in excess of 1700°C using fiber Bragg gratings," J. Opt. Soc. Am. B **30**(7), 1835 (2013).
13. A. Heptonstall, M. A. Barton, A. Bell, G. Cagnoli, C. A. Cantley, D. R. M. Crooks, A. Cumming, A. Grant, G. D. Hammond, G. M. Harry, J. Hough, R. Jones, D. Kelley, R. Kumar, I. W. Martin, N. A. Robertson, S. Rowan, K. A. Strain, K. Tokmakov, and M. van Veggel, "Invited Article: CO_2 laser production of fused silica fibers for use in interferometric gravitational wave detector mirror suspensions," Rev. Sci. Instrum. **82**(1), 011301 (2011).
14. D. A. Coucheron, M. Fokine, N. Patil, D. W. Breiby, O. T. Buset, N. Healy, A. C. Peacock, T. Hawkins, M. Jones, J. Ballato, and U. J. Gibson, "Laser recrystallization and inscription of compositional microstructures in crystalline SiGe-core fibres," Nat. Commun. **7**, 13265 (2016).
15. C. A. Lin, J. H. Chen, and L. A. Wang, "High-Q Si microsphere resonators fabricated from Si-cored fibers for WGMs excitation," IEEE Photonics Technol. Lett. **27**(13), 1355–1358 (2015).
16. G. N. Smith, K. Kalli, and K. Sugden, "Advances in Femtosecond Micromachining and Inscription of Micro and Nano Photonic Devices," in *Frontiers in Guided Wave Optics and Optoelectronics,* Bishnu Pal, ed. (InTech, 2010).
17. T. E. Glover, "Hydrodynamics of particle formation following femtosecond laser ablation," J. Opt. Soc. Am. B **20**(1), 125–131 (2003).
18. P. Liu, R. Yen, N. Bloembergen, and R. Hodgson, "Picosecond Laser-Induced Melting and Resolidification Morphology on Si," Appl. Phys. Lett. **34**(12), 864–866 (1979).
19. Y. Nissim, J. Sapriel, and J. Oudar, "Microprobe Raman Analysis of Picosecond Laser Annealed Implanted Silicon," Appl. Phys. Lett. **42**(6), 504–506 (1983).
20. Y. Kanemitsu, I. Nakada, and H. Kuroda, "Picosecond laser-induced anomalous crystallization in amorphous-silicon," Appl. Phys. Lett. **47**(9), 939–941 (1985).
21. Y. Lai, K. Zhou, K. Sugden, and I. Bennion, "Point-by-point inscription of first-order fiber Bragg grating for C-band applications," Opt. Express **15**(26), 18318–18325 (2007).
22. A. Theodosiou, A. Lacraz, M. Polis, K. Kalli, M. Tsangari, A. Stassis, and M. Komodromos, "Modified fs-laser inscribed FBG array for rapid mode shape capture of free-free vibrating beams," IEEE Photonics Technol. Lett. **28**(14), 1509–1512 (2016).
23. A. Lacraz, M. Polis, A. Theodosiou, C. Koutsides, and K. Kalli, "Femtosecond laser inscribed Bragg gratings in low loss CYTOP polymer optical fiber," IEEE Photonics Technol. Lett. **27**(7), 693–696 (2015).
24. J. J. Kaufman, G. Tao, S. Shabahang, E.-H. Banaei, D. S. Deng, X. Liang, S. G. Johnson, Y. Fink, and A. F. Abouraddy, "Structured spheres generated by an in-fibre fluid instability," Nature **487**(7408), 463–467 (2012).
25. M. Langen, T. Hibiya, M. Eguchi, and I. Egry, "Measurement of the density and the thermal expansion coefficient of molten silicon using electromagnetic levitation," J. Cryst. Growth **186**(4), 550–556 (1998).
26. K. Borzycki and K. Schuster, "Arc Fusion Splicing of Photonic Crystal Fibres," in *Photonic Crystals, Introduction, Applications, and Theory*, A. Massaro, ed. (InTech, 2012).
27. J. Bei, T. M. Monro, A. Hemming, and H. Ebendorff-Heidepriem, "Fabrication of extruded fluoroindate optical fibers," Opt. Mater. Express **3**(3), 318 (2013).
28. J. Bei, T. M. Monro, A. Hemming, and H. Ebendorff-Heidepriem, "Reduction of scattering loss in fluoroindate glass fibers," Opt. Mater. Express **3**(9), 1285–1301 (2013).
29. E. F. Nordstrand, A. N. Dibbs, A. J. Eraker, and U. J. Gibson, "Alkaline oxide interface modifiers for silicon fiber production," Opt. Mater. Express **3**(5), 651–657 (2013).
30. N. Healy, "Raman shifts of laser annealed fibers" (2016).
31. J. C. Tsang, P. M. Mooney, F. Dacol, and J. O. Chu, "Measurements of alloy composition and strain in thin GexSi1−x layers," J. Appl. Phys. **75**(12), 8098–8108 (1994).
32. L. H. Wong, C. C. Wong, J. P. Liu, D. K. Sohn, L. Chan, L. C. Hsia, H. Zang, Z. H. Ni, and Z. X. Shen, "Determination of raman phonon strain shift coefficient of strained silicon and strained SiGe," Jpn. J. Appl. Phys. **44**(11 11R), 7922–7924 (2005).
33. M. Green and M. Keevers, "Optical-properties of intrinsic silicon at 300 K," Prog. Photovolt. Res. Appl. **3**(3), 189–192 (1995).
34. K. Tsuruda, M. Fujita, and T. Nagatsuma, "Extremely low-loss terahertz waveguide based on silicon photonic-crystal slab," Opt. Express **23**(25), 31977–31990 (2015).

1. Introduction

Semiconductor core fibers have emerged recently as an interesting alternative to planar silicon for a variety of optoelectronic application [1–3]. These fibers, are produced either by high pressure chemical vapor deposition [4] or using conventional glass-fiber drawing processes [5]. Silicon-core fibers drawn from bulk preforms have been made with lengths up

Optical Materials EXPRESS

to ~100 m with core diameters down to 12 μm [6], and resonators, tapers and splices have been made of these fibers, using conventional arc-based methods.

Heating silicon-core fibers above the melting point of the core, using a hydrogen flame, leads to formation of small spheres trapped inside the glass [7]. Thermal annealing has been employed to reduce optical losses [8], and CW laser illumination using above-bandgap radiation has been used to recrystallize fiber cores [9], both for introducing high stress levels with a resulting modification of the bandgap [10] in silicon cores and for reducing optical losses in germanium [11] ones.

The entire cross-section of the fiber can be modified by appropriate choice of the laser source. Longer wavelength sources, such as CO_2 lasers, allow for localized and reproducible heating and cooling of the glass cladding and are commonly used for thermal processing of optical fibers [12] including their recent applications in gravity wave detector mirror suspensions [13]. Their use for recrystallization of the crystalline semiconductor core in both silicon [6] and SiGe-core [14] fibers has been reported, and a CO_2 laser has been used to form a silicon resonator on the exposed tip of a fiber [15].

Short-pulse visible lasers have been used extensively for the characterization of semiconductor-core fibers, but they can also be used to modify the stress at the core-cladding interface. They provide an alternative route to the traditional UV laser-induced inscription of gratings in fibers [16], offering a "direct-write" technique that is extremely flexible for producing high-resolution structures in transparent and opaque materials. The former process is typically an interaction driven through multi-photon absorption, and realized within the bulk material. Typical pulse durations are <250 fs, hence even moderate average powers can produce extremely intense laser pulses. If one accounts for the pulse duration, absorption takes place at shallower depths and the absorption coefficient dramatically increases, concomitantly increasing the temperature at the laser focus. If this occurs on a scale comparable to the optical (laser) wavelength, it is readily possible to generate extreme temperatures (10^4 – 10^5 K) at the focus [17]. However, in contrast to the CO_2 laser induced modification, the process is essentially "cold", as cooling rates are extremely high. The heat dissipation to the surroundings results in re-solidification of molten material, a process that has been shown to lead to the formation of amorphous silicon [18–20]. A significant obstacle for the realization of Bragg gratings using fs lasers, and, in particular point-by-point and line-by-line methods, is the need for precise inscription coinciding with the fiber's longitudinal axis. This is needed to maximize the overlap between the grating and guided modes; demanding significant penetration into the core material [21]. In contrast, a modified femtosecond-laser plane-by-plane FBG inscription method has been developed where two-dimensional index planes are inscribed, modifying the silicon-glass interface, and leading to stress modulation across the core [22,23].

In this paper, we demonstrate the use of a CO_2 laser for simultaneous structuring of both the semiconducting core and the silica glass cladding to form resonators and tapers, and we report inscription of Bragg gratings using visible fs pulses. These are important steps in the drive towards in-fiber photonics, as smaller cores, and wavelength-selective structures allow a wider variety of devices to be explored.

2. Experimental methods

The fibers studied here were produced using a conventional draw tower, as described in [6]. Briefly, a silica preform of 30 mm outer diameter and 3 mm coated bore was loaded with a bulk silicon rod, and heated above the softening point of the glass, well above the melting point of the silicon. Drawing down the glass formed a coaxial silicon core - silica clad fiber with 125 μm outer diameter and a 12 μm core. For tapering studies, the fiber was sleeved into a silica capillary to increase the cross-section and thus the power absorbed from the CO_2 laser beam. Thin-walled preforms were used for the fabrication of spherical resonators.

Optical Materials EXPRESS

The 30 W CO_2 laser used in these studies was controlled using 5 kHz pulse-width modulation and a ZnSe lens to vary the power. Levels used, measured behind the fiber were 5-20 W, as reported by a Thorlabs S314C detector. Programmable Aerotech stages (ALS130) with a maximum travel of 50 mm and a translation speed of up to 300 mm/s, were used to translate the fiber and the beam and to apply tension to the heated fiber for tapering. Breakup of the 12 μm core into spheres was induced with a scan rate of ~125 μm /sec, a power level (measured behind the fiber) of 12 W, and a spot size of 140 μm. 250 ms pulses at 18 W were used to change the stress on encapsulated spheres.

Taper preforms were made by sleeving a 50 μm silicon-core, 500 μm outer diameter (o.d.) fiber into a silica capillary with an inner diameter of 750 μm and an o.d. of 1750 μm; this preform was drawn down to an o.d of ~160 μm. Tapers were drawn with a preform feed rate of 100 μm/s and a draw speed of 1 cm/s, using laser powers of 12-16 W.

Raman characterization was performed using a Renishaw InVia Reflex Spectrometer System, and scanning electron imaging was performed using a Hitachi TM3000 SEM. Photomicrographs were taken with a Nikon Eclipse LV100 microscope.

All femtosecond laser inscription was undertaken using a HighQ laser (femtoREGEN) operating at 517 nm and 5 kHz, with a 220 fs pulse duration and pulse energies of 100 nJ. The fibers were mounted on Aerotech air bearing stages (ABL1000) for accurate two-axis motion; precise synchronization of the laser pulse and stage motion allowed for suitable laser processing. The laser beam was swept transversely across the core at a velocity of 50 μm/s, resulting in a mean exposure of 100 pulses/μm. The focal spot size was measured to be ~1μm. This results in an energy density approaching 100 kJ/m^2 (10 J/cm^2) at the laser focus. The fiber was displaced by a controlled step and this motion was repeated to define a periodic modulation along the fiber length. This resulted in the fabrication of a Bragg grating, which was probed in longitudinal reflection through the silicon core. The direct-write allows a wide range of spacings to be written, with a maximum length limited by our stage (100 mm). The frequency-doubled wavelength was chosen because the silica is transparent and the silicon is absorbing for this radiation, concentrating the energy at the interface region.

3. Results and discussion

3.1 CO_2 laser processing

There were three primary regimes in which the CO_2 laser treatment was conducted. In the first, the power delivered was coupled to a scan rate that permitted melting of the core without inducing Rayleigh instabilities [7,24]; this resulted in recrystallization and optical loss reduction as previously reported [6]. In the second, the scan rate was reduced or the power increased to induce controlled breakup of the core, and coalescence of large silicon particles as resonators. In the third regime, the core was melted and the glass was softened; when mechanical force was applied during treatment, tapers were formed.

3.1.1 In-fiber silicon structures

Figure 1 demonstrates the ability of the laser processing to make structures with both thin and thick glass layers and with varying dimensions. A CO_2 laser may be used to break the core into periodically spaced silicon spheres via capillary instability, comparable to those made with a flame [7], as shown in Fig. 1(a). In addition, using a fiber with a large core:clad ratio, it was possible to create large silicon spheres with a thin cladding of silica, such as that shown in Fig. 1(b). Such structures are highly responsive to temperature [8] and nonlinear optical changes [3] in the silicon, and may form the basis for sensitive detectors and fast optical switches. Compressing the glass fiber during CO_2 heating accumulates extra glass around the molten spheres that are formed, as illustrated in Fig. 1(c). This would provide axial confinement for whispering gallery modes.

Optical Materials EXPRESS

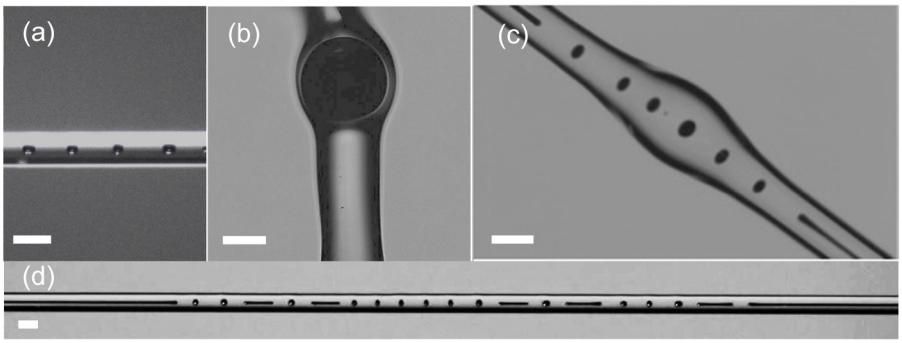

Fig. 1. Silicon structures formed by CO_2 laser processing (a) periodic array made by slow translation, (b) single sphere formed from large-core fiber (c) bottle resonator with spheres formed by compressing the fiber lengthwise during heating, and (d) aperiodic array formed by sequential heating and translation steps. Scale bars are 125 μm.

The CO_2 laser allows for the creation of a small heat zone, and variable length core sections could be made by rapid translation of the beam followed by a pause to open a gap in the core. The demonstration structure written into 12 μm core fiber, shown in Fig. 1(d) illustrates spacing of silicon structures down to ~120 μm in these fibers.

3.1.2 Stress modification of in-fiber silicon structures

The silicon cores of as-drawn fibers in this study typically exhibited tensile strain, and several factors can contribute to the final stress state of silicon structures in glass. Silicon undergoes a large expansion upon solidification, yet also has a thermal coefficient of expansion that is much larger than that of the silica cladding.

The density of liquid silicon near the melting point of 1414 °C has been experimentally measured to be 2.52 g/cm^3 [25], while that of crystalline silicon at these temperatures is close to 2.3 g/cm^3, implying an expansion of about 4% in each dimension upon solidification, which would lead to an expectation of compressive stress in the core. However, if the glass accommodates the initial expansion of the silicon, the difference in the thermal expansion coefficient (silicon~2.6×10^{-6} K^{-1}, silica ~0.6×10^{-6} K^{-1}) during cooling, will lead to tensile strain in the core at room temperature. During the drawing process, the solidification front moves unidirectionally, pushing the liquid ahead of the solid, thus allowing unconstrained expansion, and the subsequent contraction during cooling dominates the strain at room temperature.

Additional considerations in the stress/strain picture include the fact that the viscosity of the glass at the melting point of silicon (~10^9 Pa-s [26]), is in the range used for glass extrusion processes [27,28], above the glass transition temperature, implying significant stress/strain relaxation. The silicon-silica interface is modified with an oxide to reduce stress during solidification [29], and this layer may reduce the viscosity at the interface region further.

When the silicon is fully encapsulated, the unidirectional relief mechanism is no longer active, and compressive stress can be introduced since the lattice expansion upon silicon solidification is approximately a factor of ten larger than the contraction during cooling from the melting point to room temperature. This will be especially true if the time available for flow of the glass is limited, as will occur during rapid cooling. Increasingly compressive strains are seen as the translation speed is increased during resolidification of silicon fibers [30].

Optical Materials EXPRESS

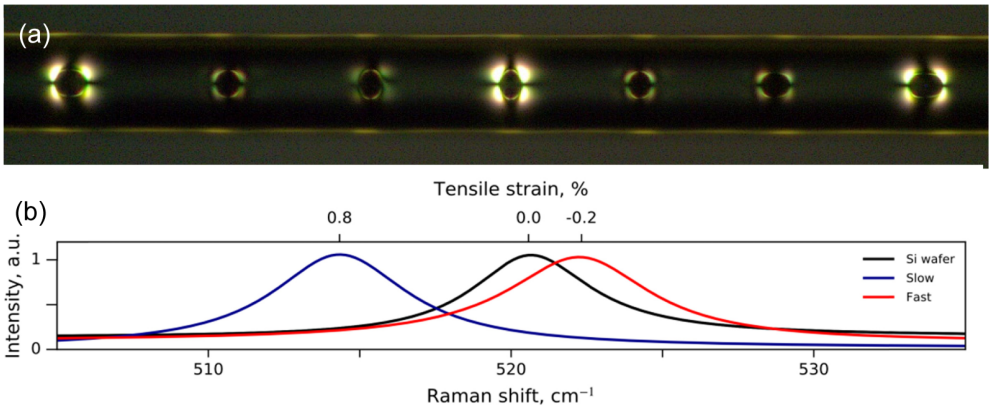

Fig. 2. (a) Birefringence around silicon spheres encased in a 125 µm glass fiber. Every third sphere was exposed to a high power pulse of CO_2 radiation, causing remelting and rapid resolidification. A fast cooling rate is correlated with high birefringence, and (b) changes in the Raman shift of the silicon. Black line is the reference wafer, blue line is a slowly cooled sphere and red is for the sphere with the highest cooling rate.

The effect of cooling on a series of silicon spheres was used to explore this phenomenon, and the results were characterized by microscopy through crossed polarizers and by Raman spectroscopy. Tensile strain in silicon results in shifts in the position of the main Si peak at 520.5 cm^{-1} towards lower wavenumbers, with a strain of 1% leading to a change of 7.05 cm^{-1} [31] to 7.84 cm^{-1} [32]. We found that as the cooling rate is increased, the residual strain becomes less tensile. Figure 2(a) shows the birefringence for a fiber where the laser was shuttered to treat every third sphere to a high power pulse, melting the sphere, and cooling rapidly. Raman results for different treatments are shown in Fig. 2(b). For the untreated fiber, the silicon peak was at 512 cm^{-1}, indicating a tensile strain of ~0.82%. After formation of the spheres at peak temperatures just above to the melting point of silicon, there was typically a residual but reduced tensile stress, with measured shifts of 514 ± 1 cm^{-1} (Fig. 2(b), blue curve). Opening the shutter at 18 W for 250 ms during scanning, estimated to give a peak temperature of 1650 °C [6] caused the spheres to melt and resolidify during translation, leading to a Raman shift of 520 cm^{-1}. In this case there is near cancellation of the compression due to solidification and the tension associated with differential thermal contraction during cooling. A 2-3 s exposure to the 18 W beam was sufficient to cause deformation of the fiber, with a temperature estimated to be >1900 °C, followed by rapid cooling after the shutter was closed. In this case, (Fig. 2(b), red curve), the Raman peak was at 522.3 cm^{-1}, indicating that significant residual compressive strain can be developed. This supports a viscoelastic model in which there is an accommodation of the silicon expansion upon solidification due to stress/strain relaxation during slow cooling conditions, while rapid cooling restricts glass relaxation, resulting in a residual compressive component.

3.1.3 Laser tapering of silicon-core fibers

The CO_2 laser permits softening of the glass and rapid melting of the silicon core so that if tension is applied to the fiber during heating, the fiber can be tapered. In addition to redrawing the fiber from a fixed heated spot, it is possible to set a feed rate for the fiber into the beam, while pulling on one end, analogous to the way that a fiber is initially drawn from a preform. This permits the fabrication of a taper followed by a long (several mm) section of the fiber with a reduced core size, as shown in Fig. 3(a). Both adiabatic [14] and abrupt tapers can be formed using this approach. During tapering, the reduction in cross-section of the fiber results in reduced absorption of CO_2 laser radiation, setting a limit to the attainable core dimension. Fibers were prepared by sleeving into a silica capillary to give a higher-than

Optical Materials EXPRESS

standard ratio of glass to silicon core diameter. The resultant fiber tapers had a 1.5 μm core, as shown in Fig. 3(b), from a single step tapering process. Imperfect matching of the capillary and fiber dimensions led to a gap between the two silica layers that is not present in most fibers. Raman spectroscopy (Fig. 3(c)) on the exposed end of the silicon core shows a shift of 518.3 cm^{-1}, a reduction of tensile stress compared to the unprocessed fiber core. Measurement of the Raman shift along the rapidly decreasing portion of the diameter at the taper end shows that the stress becomes less tensile as the diameter decreases. As the cooling rate is fastest for the smallest diameter, this again supports the observation that rapid cooling is associated with reduced accommodation of the silicon expansion.

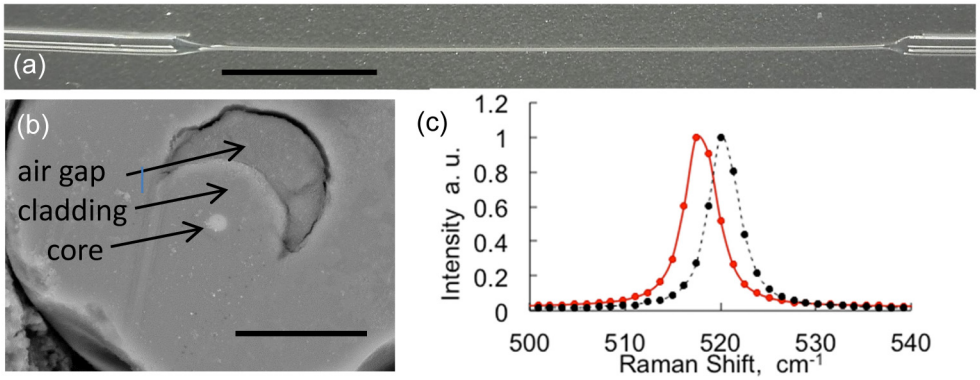

Fig. 3. Silicon tapers: (a) Photograph of 4mm long taper produced with a 125 μm fiber sleeved into a silica capillary (scale bar 1mm), (b) cross-section of the core after drawing (scale bar 10 μm). The moon shaped region is a cavity formed in the sleeving process due to mismatch of the capillary and fiber diameters. (c) Raman spectrum from the exposed face of the core (solid red curve) and reference silicon wafer (dashed black curve).

3.2 Femtosecond laser processing

CO_2 laser processing modifies the fibers by heating the glass cladding, with conductive heat transfer to the core. Continuous wave visible radiation passes through the glass, and interacts strongly with the core material, and this has been used to recrystallize semiconductor cores [10,11]. Ultrashort pulses at a wavelength of 517 nm, however, can be used to introduce strain within the cladding and at the interface between the glass and the core without significantly affecting the properties of the core material; the penetration depth in silicon at this wavelength is limited to ~1μm, corresponding to an absorption coefficient of ~0.9 μm^{-1} [33]. In these preliminary experiments, a 12 μm core fiber previously recrystallized at a scan rate of 3 mm/s (to reduce optical losses) [6] was exposed at the core/clad interface as described in section 2 above.. During the inscription process, strong plasma generation in the region of the Si core was observed (see Fig. 4(a) inset) as the laser swept across the core.

The period of the modulation of the core region was set to Λ = 1820 nm using the programmable stages, corresponding to an 8th order grating; where a silicon refractive index value of 3.441 would result in a grating close to a wavelength of 1565 nm. Figure 4(a) shows the spectrum from a 2000-plane grating with a target grating response at 1.565 μm, which results in a reflected linewidth of ~0.9 nm. To the best of the authors' knowledge, this is the first Bragg grating written into a silicon optical fiber. In addition to the expected grating reflectivity, significant stress changes are observed by both birefringence in the glass, and Raman shifts in the core material resulting from the grating fabrication.

Optical Materials EXPRESS

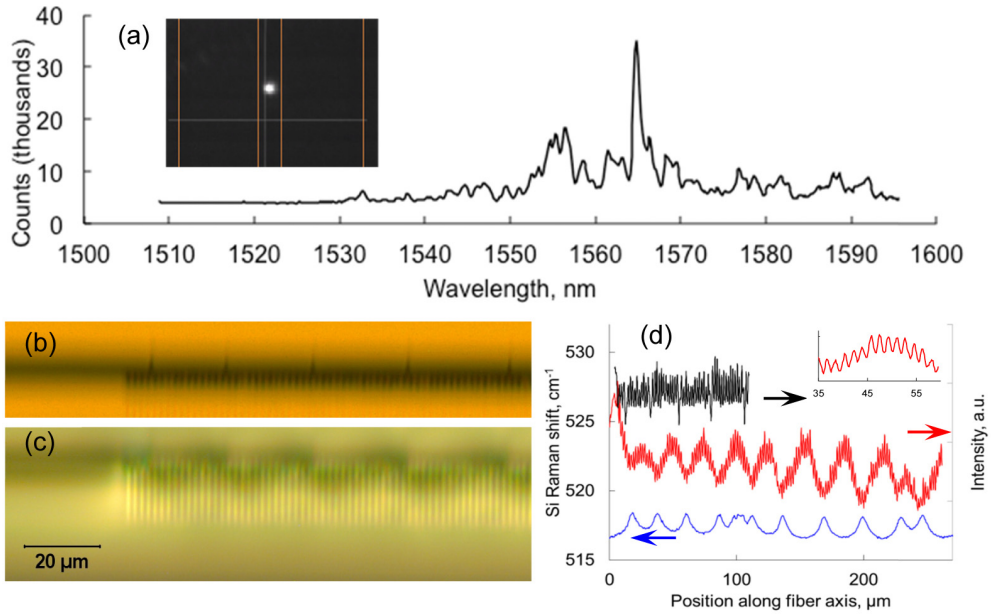

Fig. 4. (a) Reflection spectrum from a 2000-plane grating written in the interface region of the silicon-core fiber. Inset shows a darkfield image of the plasma created during inscription (lines indicate edges of core and cladding). (b) Transmission image of fiber grating showing 1.8 µm period and additional features with a spacing of ~20 µm. (c) Image of the same region through partially crossed polarizers, showing variations in the stress-induced birefringence. (d) scans of the intensity vs. position along the images in (b) (black curve) and (c) (red curve), along with the Raman shift (blue curve) of the silicon peak plotted on the same axis. Inset shows an expanded region of (c) revealing the grating period. There is a clear correlation between the crack-like features, the birefringence in the glass and the residual strain in the silicon.

Figure 4(b) is a microscope image of one end of the grating region, using transmitted light, showing the grating period, as well as some sharp aperiodic features extending away from the grating region. Figure 4(c) is the same part of the fiber imaged through crossed polarizers; the color variations are due to birefringence. The grating lines, as well as quasi-periodic variations in the stress-induced birefringence can be seen. Figure 4(d) shows intensity plots from the micrographs together with the Raman shift of the silicon peak as a function of position in the same region. The Raman curve was generated by measuring the Raman spectrum every 0.5 µm, and plotting the position of the Si peak (in cm^{-1}) as a function of position along the fiber. It should be noted that the lateral resolution of the Raman measurement is ~4 µm, so stresses associated with the grating period could not be resolved. There is a clear overall increase in the compressive strain in the vicinity of the grating, and quasi-periodic Raman shift changes that correlate with the larger features in Fig. 4(a), suggesting possible strain relief through the formation of microcracks. It is possible that illumination with a CO_2 laser during fs exposure, at a power sufficient to soften the glass but not to melt the core, might permit elimination of the cracks. Writing the grating in sections may also reduce damage.

4. Conclusion

Laser processing is a versatile technique for modifying the structure of semiconductor-core glass fibers. Here, modification of the core shape, structure and stress properties has been demonstrated through both infrared and visible laser processing.

Stress control of semiconductor-in glass structures created by Rayleigh instability suggests a novel way to manipulate the band structure, and possibly realize direct gaps and

Optical Materials EXPRESS

light emission in group IV materials such as germanium-tin alloys, and FBG formation opens a route to fiber-based silicon Raman lasers. Fibers with these core materials could also be stressed directly by fs processing.

Silicon also is an attractive material for the formation of photonic crystals for THz radiation, and 2-d structures have been reported to have low losses [34]. Photonic crystal arrays for long wavelengths could be made by forming the desired periodic or aperiodic structure as illustrated in Fig. 1(d) inside a large number of fibers; these fibers could then be placed side-by side to form a layer, and a 3-d array could be built by stacking many layers. This would allow a bottom-up approach to constructing photonic crystals with considerable design freedom.

Funding

Support for this work was provided by The Norwegian Research council grants 219686/O70 and 262232/O70 and the Norwegian Micro-and Nano-Fabrication facility, NorFab, project number 245963/F50, as well as the Stiftelsen för Strategisk Forskning (SSF) grant RMA15-0135, and the Knut and Alice Wallenberg Foundation (KAW) grant 2016.0104. The J. E. Sirrine Foundation also is gratefully acknowledged for support.